Multi-Node Open-Loop Distributed Beamforming Based on Scalable, High-Accuracy Ranging

Sean M. Ellison, *Member, IEEE*, Serge R. Mghabghab, *Student Member, IEEE*, and Jeffrey A. Nanzer, *Senior Member, IEEE*

***Abstract*—We present a distributed antenna array supporting open-loop distributed beamforming at 1.5 GHz. Based on a scalable, high-accuracy internode ranging technique, we demonstrate open-loop beamforming experiments using three transmitting nodes. To support distributed beamforming without feedback from the destination, the relative positions of the nodes in the distributed array must be known with accuracies below $\lambda/15$ of the beamforming carrier frequency to ensure that the array maintains at least 90% coherent beamforming gain at the receive location. For operations in the microwave range, this leads to range estimation accuracies of centimeters or lower. We present a scalable, high-accuracy waveform and new approaches to refine range measurements to significantly improve the estimation accuracy. Using this waveform with a three-node array, we demonstrate high-accuracy ranging simultaneously between multiple nodes, from which phase corrections on two secondary nodes are implemented to maintain beamforming with the primary node, thereby supporting open-loop distributed beamforming. Upon movement of the nodes, the range estimation is used to dynamically update the phase correction, maintaining beamforming as the nodes move. We show the first open-loop distributed beamforming at 1.5 GHz with a three-node array, demonstrating the ability to implement and maintain phase-based beamforming without feedback from the destination.**

***Index Terms*—Coherent distributed arrays, cooperative ranging, disaggregated arrays, distributed antenna arrays, distributed beamforming, radar**

I. Introduction

Progress in wireless communications systems, as well as other wireless applications such as remote sensing, radar, and imaging, depends on the ability to continually improve the capabilities of antennas, arrays, and transceivers in terms of power, gain, throughput, and resolution, among other metrics. Improvements in these metrics are often achieved by focusing on new individual components and subsystems, resulting in better individual platform-based systems. However, limitations of this platform-centric model, stemming from constraints on size, weight, cost, and power consumption, make it increasingly challenging to scale such performance metrics on a single platform. To address this challenge, recent research has focused on the development of distributed wireless technologies, where collections of small, relatively inexpensive wireless systems are coordinated to mimic the performance of a single, large system, or to achieve performance otherwise unattainable with a single platform. Implemented in Multiple Input Multiple Output (MIMO) [1]–[6] or distributed beamforming [7]–[12] applications, such distributed wireless systems enable direct performance scalability by adding or removing inexpensive nodes from the array [13], [14].

Coherent distributed arrays (CDAs) are a particular form of distributed wireless system where individual wireless elements coordinate at the level of the radio frequency (RF) phase to enable distributed beamforming [9], [15], [16]. Coordination of separate moving nodes is a challenging problem, in which the following three fundamental coordination tasks must be accomplished: frequency synchronization to ensure all elements are operating at the same reference frequency [17]–[20]; time alignment to ensure that there is sufficient overlap of the information at the target destination [21]–[23]; and phase alignment to enable constructive interference at the target. Phase alignment presents the most challenges due to the extremely small tolerance to errors at microwave frequencies. Past works approached this issue through closed-loop feedback loops where a receiver co-located with the target location provides information to the transmitting array, from which the transmitters can determine how to adjust their relative phases to converge to a phase-coherent state at the receiver. Among these closed-loop approaches are one-bit feedback [24], [25], three-bit feedback [26], primary-secondary synchronization [9], receiver-coordinated explicit-feedback [27], reciprocity where channel estimation is performed from signals sent by the target receiver [28], [29], round-trip synchronization [30], and two-way synchronization [31]. Although these feedback methods are effective, they are restricted to applications where reliable feedback can be provided by the destination. Numerous situations arise where such feedback is not available, particularly in cases where individual nodes in the array do not have sufficient sensitivity to close a link to a base station on their own. Furthermore, closed-loop architectures are inherently unable to support wireless applications beyond communications, such as remote sensing, imaging, and radar where coherent feedback is generally not present.

Manuscript received 2020.

This material is based in part upon work supported by The Defense Advanced Research Projects Agency under grant number N66001-17-1-4045, the National Science Foundation under grant number 1751655, and by the Air Force Research Laboratory under contract number FA8650-14-D-1725. The views, opinions, and/or findings contained in this article are those of the author and should not be interpreted as representing the official views or policies, either expressed or implied, of the Defense Advanced Research Projects Agency or the Department of Defense. *(Corresponding Author: Jeffrey A. Nanzer)*

S. M. Ellison was with the Department of Electrical and Computer Engineering, Michigan State University, East Lansing, MI 48824 USA. He is now with the Johns Hopkins University Applied Physics Laboratory, Laurel, MD, 20723 (e-mail: sean.ellison@jhuapl.edu)

S. R. Mghabghab and J. A. Nanzer are with the Department of Electrical and Computer Engineering, Michigan State University, East Lansing, MI 48824 USA (e-mails: mghabgha@msu.edu, nanzer@msu.edu).

In this work, we present what is, to the best of our knowledge, the first open-loop distributed beamforming system using a scalable, high-accuracy ranging waveform with more than two transmitting nodes. The ranging waveform is based on a two-tone stepped-frequency waveform that supports ranging to multiple nodes simultaneously. We demonstrate the use of this waveform in an open-loop distributed transmitter array consisting of three separate 1.5 GHz transmitters. One node is designated as the primary node, with the two additional secondary nodes performing high-accuracy ranging from which the secondary nodes implement a phase-coherent transmission to cohere at a separate receiver. We demonstrate coherent signal summation at end-fire orientation that is maximally impacted by range-induced phase errors and thus represents the most challenging beamforming case. The results of this work may be combined with wireless frequency synchronization techniques [17]–[20] for fully wireless beamforming. In Section III we describe the waveform parameters associated with internode localization followed by Section III-A where the hardware setup associated with both the primary and secondary nodes is discussed. Section IV reviews the tolerance of gain degradation due to errors in position and explores the inherent uncertainty that is present in the localization waveform. Methods for improvement in localization, such as retransmit gain from the primary, matched filtering, interpolation, and Kalman filtering, and are discussed in Section V followed by a discussion of the measurements incorporating dynamic phase shifting to implement distributed beamforming.

II. Open-Loop Distributed Beamforming Model

Open-loop CDAs (i.e. feedback-free distributed arrays) are types of CDAs where feedback from the destination location is not leveraged, thus the array self-coordinates to a phase-aligned state [16], [32]. To achieve phase alignment and implement a phase-based beamsteering operation, the relative positions of the individual nodes must be known to within a fraction of the wavelength of the beamforming frequency. Previous works have shown that these internode ranging measurements must have accuracies of less than $\lambda/15$ to have no more than 0.5 dB reduction in coherent gain with a probability of 90% [16], [33]. To operate in the microwave range this calls for accuracies on a sub-centimeter level. Furthermore, this accuracy must be obtained before the nodes move out of coherence due to array dynamics. This has been achieved in the past using optical systems but such systems are not easily scalable and require accurate tracking and pointing for each node connection [34]–[36]. We have previously shown that spectrally-sparse waveforms can achieve near-optimal ranging accuracy, and can be designed to support simultaneous ranging between multiple nodes, while using a microwave link that does not require accurate pointing and tracking [37]. This method of phase adjustment through localization for open-loop arrays presents a much more general approach than that of closed-loop systems, enabling applicability to situations where array gain is necessary to initialize the link and to sensing applications where coherent feedback is not available.

The received signal in the far field from an array of N arbitrarily placed transmitting nodes can be represented by

$$s_r(t) = \sum_{n=1}^{N} h_n A_n(t - \delta t(n)) e^{j[2\pi(f+\delta f(n))t + \phi_{s,n} - \phi_{c,n} + \delta\phi(n)]} \tag{1}$$

where h_n is the complex valued coefficient representing the propagation channel between the destination and the nth node, which includes multipath impacts and antenna phase differences, A_n is the signal amplitude of the nth signal, $\delta t(n)$ represents the timing error, f is the nominal center frequency, $\delta f(n)$ is the frequency error, $\phi_{s,n}$ is the phase shift, $\phi_{c,n}$ is the correction applied to the phase shift which can be obtained through nodes localization, and $\delta\phi(n)$ is the instantaneous frequency and phase errors which is the result of multiple factors. Of the many factors that impact distributed beamforming performance, the ability to accurately estimate the necessary internode phase to achieve coherent summation of the transmitted signals to a desired angle is among the most fundamental. A number of prior works have focused on time alignment and frequency transfer, as noted above; here, we focus on the ability to estimate the necessary phase between nodes to achieve coherent beamforming from measurements of the internode range. This represents a fundamental coordination aspect that is necessary for open-loop distributed beamforming. In coordination with other approaches for time and frequency synchronization, the work herein represents a foundation for open-loop distributed beamforming systems. In presence of beamforming phase errors derived from estimating the internode range, the received signal model (1) can be reduced to

$$s_r(t) = C \sum_{n=1}^{N} e^{j(2\pi f t + \phi_{s,n} + \phi_n)} \tag{2}$$

where $C = \sum_{n=1}^{N} h_n A_n(t)$, and $\phi_{s,n}$ is the delay imparted at node n by the node separation, given by

$$\phi_{s,n} = 2\pi f \tfrac{d_n}{\lambda} \cos\theta, \tag{3}$$

$\lambda = \frac{c}{f}$ is the wavelength with c the speed of light; and ϕ_n is the phase correction with errors given by

$$\phi_n = \frac{2\pi}{\lambda}(d_n + \delta d_n)\cos\theta_n \tag{4}$$

where δd_n is error in localization, θ_n is the error in beamsteering angle. Here we consider the most challenging case in terms of ranging errors with end-fire beamforming, where $\theta_n = 0$ and thus $\phi_n = \frac{2\pi}{\lambda}(d_n + \delta d_n)$.

A perfectly aligned system would produce an ideal signal given by

$$s_i(t) = C \sum_{n=1}^{N} e^{j\left(2\pi f t - \frac{2\pi}{\lambda} d_n\right)}. \tag{5}$$

To evaluate the effects of localization errors on the power of the beamformed signal, the power of the signal with errors (2) is evaluated relative to that of the ideal signal (5) by

$$G_c = \frac{|s_r s_r^*|}{|s_i s_i^*|} \tag{6}$$

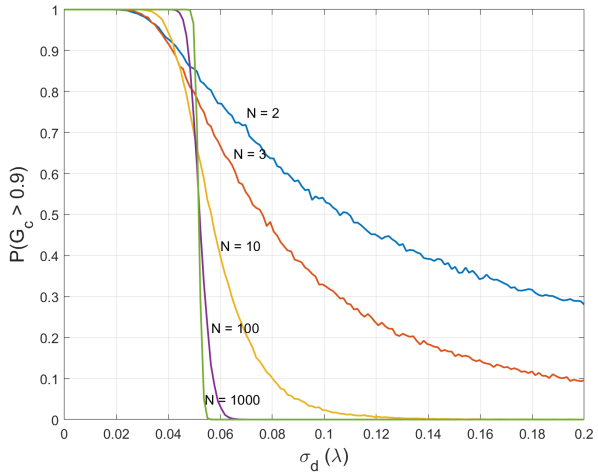

Fig. 1. Probability of obtaining coherent gain above 90% ($P(G_C \geq 0.9)$) for various array sizes versus standard deviation of internode range error for the special case of end-fire configuration. As array becomes large, the threshold for $P(G_C \geq 0.9) = 1$ approaches $\lambda/20$.

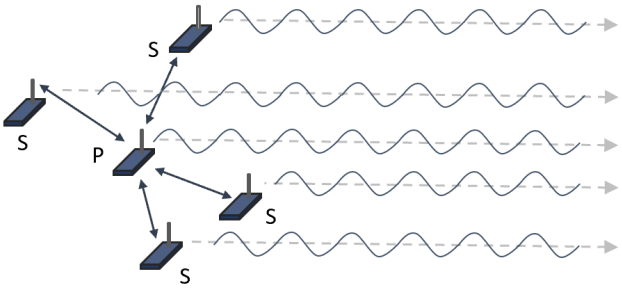

Fig. 2. Distributed antenna array topology using a primary-secondary ranging approach.

The standard deviation of the error term σ_d was varied and the probability of exceeding a particular threshold $P(G_C \geq X)$, where $0 \leq X \leq 1$, was determined through 100,000 Monte-Carlo simulations. In this work we consider the coherent gain to be greater than 90% of that of the ideal array ($X = 0.9$). We previously showed that as the array size increases, obtaining $P(G_C \geq X)$ requires ranging errors of $\lambda/15$ or less for arbitrary steering angles [16], [33]. For the more stringent end-fire case, this requirement is closer to $\lambda/20$, as shown in Fig. 1, where the result of 10,000 Monte Carlo simulations is shown for $P(G_C \geq 0.9)$. For microwave and millimeter-wave beamforming frequencies, this requirement leads to ranging accuracies on the order of mm.

III. Range Estimation Waveform

The array design in this work is based on a primary-secondary internode ranging architecture. A diagram of this type of array design can be seen in Fig. 2. Because the relative ranges between nodes is of importance, each node in the array must perform a ranging measurement between another node such that the array forms a connected graph. Each node can then implement a beamforming operation in a pair-wise manner [16]. After estimating the baseline d between the nodes, the phase at the node performing the measurement is updated by

$$\phi_s = 2\pi f \frac{d}{\lambda} \cos\theta, \tag{7}$$

In this work, we demonstrate coordination in a linear array; extensibility to general array layouts further requires estimation of the angle of each secondary node to the primary. Angle-of-arrival (AOA) methods have been explored in literature [38], the most notable of which are MUSIC [39] and ESPRIT [40]. We focus exclusively on the ranging challenge in this work, however additional error terms that arise from angle estimation along with beamforming to arbitrary directions can be included in a total error budget [16].

To address the internode ranging (i.e. the term d in (7)), we previously investigated the use of spectrally-sparse waveforms for high-accuracy ranging, showing that a two-tone waveform obtains near-optimal ranging accuracy [41], [42]. Addressing the ambiguity challenges with a simple two-tone waveform, we previously investigated scalability approaches by developing a two-tone stepped-frequency waveform (TTSFW) [37], however it was found that the range estimates from direct matched-filtering of the ranging waveform varied upon relatively fast movement of the nodes with a magnitude too great for reliable beamforming. This work expands on prior work by implementing a Kalman filter to improve the robustness of the range measurement, and demonstrating the ability to maintain a steered beam when the nodes are moved.

The TTSFW waveform consists of a two-tone waveform that is pulse-modulated, with a change in carrier frequency in each successive pulse. The baseband waveform can be written as

$$s(t) = \frac{1}{N} \sum_{n=0}^{N-1} \text{rect}\left(\frac{t - nT_r}{T}\right) \left(e^{j2\pi f_1 t} + e^{j2\pi f_2 t}\right) e^{j2\pi n \delta f t} \tag{8}$$

where f_1 is the lower of the two tones per pulse, f_2 is the upper tone, δf is the frequency step, N is the number of pulses, T is the waveform duration, and T_r is the active portion of the pulse (i.e. T multiplied by the duty cycle). The frequency step can be given by

$$\delta f = \frac{BW}{2N - 1} \tag{9}$$

where BW is the total waveform bandwidth. The upper frequency in each two-tone pulse is then given by $f_2 = f_1 + \Delta f$ where

$$\Delta f = N \delta f \tag{10}$$

The waveform is generated such that $N!$ is greater than or equal to the number unique connections between the primary and all secondary nodes in the array. This ensures that every secondary node has a unique pulse signature, which allows for simultaneous measurements utilizing the same bandwidth with minimal interference. This baseband waveform is then upconverted to a carrier frequency f_c, which is in general different from the beamforming carrier frequency f.

In the case of a two-node array, consisting of a primary node and a single secondary node, only a single pulse $N = 1$

is required since only a single unique connection is made. Fig. 3 shows an example implementation of this waveform in the time and frequency domains. For this case the baseband waveform had a duration of 1 ms with a 50% duty cycle and frequencies $f_1 = 500$ kHz and $f_2 = 11.5$ MHz, which matches the bandwidth that has been demonstrated to obtain high ranging accuracy [37].

In the case of a three-node array, consisting of a primary node and two secondary nodes, there are two unique connections and therefore a multipulse system is required such that $N \geq 2$. We demonstrate here a waveform supporting more than three nodes, with $N = 5$ to illustrate the scalability. An image of the waveform in the time domain and frequency domain can be seen in Fig. 3. The time duration of the baseband waveform was 200 μs per pulse with a 50% duty cycle, frequencies $f_1 = 500$ kHz and $f_2 = 5.5$ MHz, and a step sized of $\delta f = 1$ MHz. To ensure that each connection has a unique pulse signature, one secondary node begins its waveform with the pulse containing the lowest frequency pair of tones and then increases the frequencies by the frequency step, while the second secondary node begins with the pulse with the highest frequency pair and then decreases the frequencies by the frequency step. The pulse labels in Fig. 3(b) given by Pulse $a - b$ indicate the pulse order relative to the secondary nodes such that the index a is associated with secondary node one while b is associated with secondary node two. This approach to unique pulse-to-pulse signatures per node is easily extendable: each secondary node is assigned a unique permutation of the pulse sequence, e.g. $\delta f \rightarrow 4\delta f \rightarrow 2\delta f \rightarrow 3\delta f \rightarrow 5\delta f$. The secondary node applies its matched filter to this stepped frequency sequence. The approach thus supports $N!$ connections for each primary node. Generally, two-tone ranging waveforms suffer from high time-sidelobes, leading to challenges with disambiguation [43]. However, the TTSFW inherently disambiguates the N nearest sidelobes [37], making disambiguation a less challenging prospect. In this work, no additional disambiguation methods were necessary, however, implementations with fewer pulses may require additional processing.

A. Ranging Requirements for Open-Loop Distributed Beamforming

Inherent uncertainly is present in any system that attempts to estimate a parameter due to the presence of random noise. A measure of the lower bound on the variance or stability of an unbiased estimate of a random variable is given by the Cramer-Rao Lower Bound (CRLB), which for time delay estimation is given by [41]

$$\text{var}(\hat{\tau} - \tau) \geq \frac{1}{\frac{2E}{N_0}\left(\zeta_f^2 - \mu_f^2\right)} \tag{11}$$

where E is the signal energy, N_0 is the noise power per unit bandwidth, ζ_f^2 is the second moment of the frequency spectrum or the mean-squared bandwidth of the waveform, and μ_f^2 is the first moment of the frequency spectrum. The term $E/N_0 = T_r \times BW_n \times \text{SNR}$, where T_r is the non-zero time duration of a ranging pulse, BW_n is the noise bandwidth,

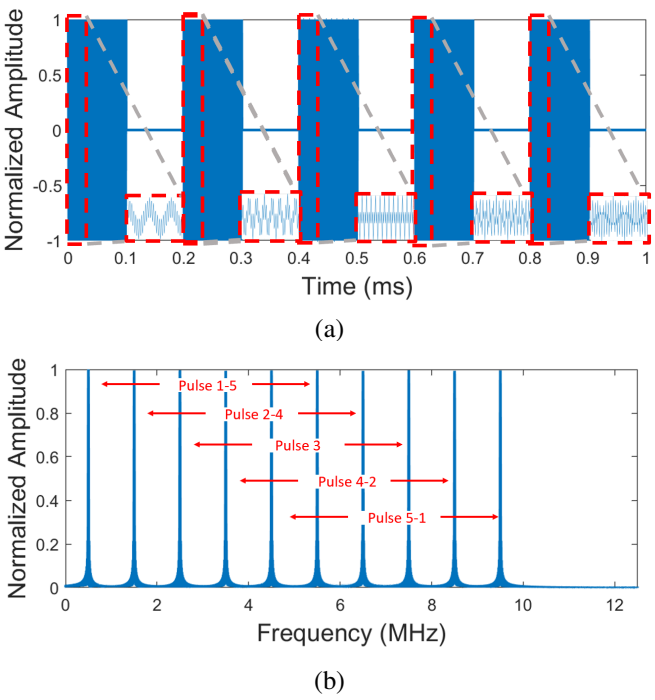

Fig. 3. Measured waveform supporting ranging between five nodes: (a) time domain; (b) frequency domain.

and SNR is the preprocessing signal-to-noise ratio. Since that the spectrum of the TTSFW is symmetric about the mean, μ_f^2 is zero. The time delay variance (11) can be converted to the two-way range variance by

$$\text{var}(\hat{x} - x) \geq \frac{c^2}{\frac{8E}{N_0}\zeta_f^2} \tag{12}$$

where the factor of 4 derives from the two-way propagation seen by typical radar measurements. Thus, (12) gives a measure of the minimum amount of positional variability that can be obtained for a given waveform. For a given SNR, the achievable variance is directly dependent on the mean-squared bandwidth, given by [41]

$$\zeta_f^2 = \frac{\int_{-\infty}^{\infty}(2\pi f)^2|S(f)|^2 df}{\int_{-\infty}^{\infty}|S(f)|^2 df} \tag{13}$$

where $S(f)$ is the spectrum content of the waveform. This can be derived for the TTSFW as [37]

$$\zeta_f^2 = \pi^2\left(\frac{BW}{2 - \frac{1}{N}}\right)^2 + \frac{(2\pi BW)^2}{N(4N^2 + 4N + 1)}\sum_{n=0}^{N-1} n^2 \tag{14}$$

For a given number of pulses N, ζ_f^2 is maximized when the bandwidth BW is also maximized and thus providing the minimum variance. This is the driving motivation behind spectrally sparse waveforms as a method for localization. The mean-square bandwidth for the two waveforms described in Section III can be derived as

$$\zeta_{f,2\text{ node}}^2\Big|_{N=1} = \pi^2 BW^2 = 1.942 \times 10^{15} \tag{15}$$

$$\zeta_{f,3\text{ node}}^2\Big|_{N=5} = \frac{507\pi^2 BW^2}{1000} = 6.0547 \times 10^{14} \tag{16}$$

We evaluate the lower bound on delay estimation for the two waveforms considering an SNR of 30 dB; this closely matches the SNR in typical cooperative ranging measurements in distributed arrays. We note that, unlike a traditional radar ranging measurement which undergoes propagation losses in both directions, the cooperative ranging implemented in a distributed antenna array only suffers losses in one direction, since the primary node is repeating the signal with gain. Thus, relatively high SNR values are feasible. The processing gain resulting from the matched filter process, a method for time delay estimation, is equivalent to the time-bandwidth product of NT_rBW_n, where N is the number of pulses in TTSFW. Since no additional filtering outside the analog bandwidth of the system is used, BW_n is equal to the sampling rate 25 MHz. If the received signals are processed with a carrier frequency offset f_0, which may be an intermediate frequency after heterodyne downconversion, the CRLB is modified by $\zeta_f^2 \rightarrow \zeta_f^2 + \zeta_{f_0}^2$, where $\zeta_{f_0}^2 = (2\pi f_0)^2$ in (14), (15), and (16). The center frequency of the sampled ranging waveform in this work has an intermediate frequency offset of $f_0 = \frac{f_1+f_2}{2}$. For $f_1 = 500$ kHz and $f_2 = 11.5$ MHz, $\zeta_{f_0}^2 = 1.421 \times 10^{15}$, theoretically reducing the CRLB by about half. However, the term $\zeta_{f_0}^2$ is dependent on the offset frequency of the sampled received signal, and thus requires higher SNR to unambiguously estimate with high accuracy. Generally, the bandwidth factor ζ_f^2 determines the lower bound for moderate SNR [44].

In the experiments discussed later, we used $T_r = 250$ μs in a two-node measurement, thus the processing gain was 38 dB resulting in a post processing SNR of 68 dB. Using (11), the bound on the variance of the time delay can be derived as $\sigma_\tau^2 = 3.059 \times 10^{-23}$ s^2 which can be converted to the two-way distance standard deviation of $\sigma_x = 830$ μm. The distance uncertainty sets the maximum operation frequency that can be achieved by

$$f \leq \frac{c}{20\sigma_x} \tag{17}$$

where σ_x is the standard deviation of the two way distance measurement and the factor of 20 derives from the coherent gain statistical analysis for the end-fire array configuration. For this case the resulting maximum frequency limit is $f_{2 \text{ node}} \leq 18.08$ GHz. For experiment conducted using three nodes, NT_r resulting from the summation of all the pulses was equal to 500 μs, yielding a processing gain of 41 dB resulting in a post processing SNR of 71 dB. The bound on the variance of the time delay was thus $\sigma_\tau^2 = 1.974 \times 10^{-23}$ s^2, and the distance standard deviation $\sigma_x = 666$ μm. The maximum operational frequency for the three node is thus derived to be $f_{3 \text{ node}} \leq 22.51$ GHz.

In practice, these estimated lower bounds are not usually achievable due to many factors such as discretization-related errors, interpolation errors, system imperfections, and interference, among others. Experimental measurements of the ranging accuracy yielded a distance standard deviation for a two-node system (one pulse) equal to $\sigma_x = 950$ μm, which allows a maximum frequency limit of 15.79 GHz. For a three-node system (two pulses), the measured ranging standard deviation was $\sigma_x = 850$ μm , which allows a maximum frequency limit of 17.65 GHz.

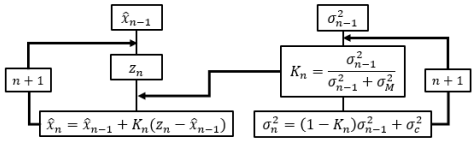

Fig. 4. Block diagram of the Kalman filter used for range estimation refinement with moving nodes (values are specified in the main text).

IV. Range Estimation Refinement for Node Motion

Phase alignment of the operational frequencies to produce a phase coherent signal at the target destination is done by estimating the range between the primary node and the corresponding secondary node and applying the appropriate phase shift. For this experiment, the ranging signals are transmitted from the secondary node(s) to the primary node where a repeater captures the signals, amplifies them, and retransmits them back. The center frequencies of the transmit and receive of the repeater are separated by 1 GHz. By doing this, the propagation losses are proportional to $1/R^2$ rather than $1/R^4$ which is seen by typical radar measurements. This will also ensure that the desired signal will dominate any multipath and most of the crosstalk can be neglected. After the ranging signal is received, the secondary node estimates the time of flight by matched filtering the return signal. The peak of the matched filter is spline interpolated in real-time in LabVIEW with a thousand points to improve the accuracy.

The matched filter output peak value is tracked using a 1-D Kalman filter. A Kalman filter gives the optimal state estimation for linear systems in the presence of Gaussian noise [45]. The model of the filter, shown in Fig. 4, is

$$\hat{x}_n = \hat{x}_{n-1} + K_n(z_n - \hat{x}_{n-1}) \tag{18}$$

where $\hat{x}_n$ is the prediction of the current state, $\hat{x}_{n-1}$ is the prediction of the previous state, z_n is the measurement at the current state, and K_n is the current state Kalman gain given by

$$K_n = \frac{\sigma_{n-1}^2}{\sigma_{n-1}^2 + \sigma_M^2} \tag{19}$$

where σ_{n-1}^2 is the previous state uncertainty and the measurement variance $\sigma_M^2 = 3 \times 10^{-5}$ is determined by measuring the variance of 1000 peak values. The current state uncertainty is then updated by

$$\sigma_n^2 = (1 - K)\sigma_{n-1}^2 + \sigma_c^2 \tag{20}$$

where an additional constant uncertainty of $\sigma_c^2 = 5 \times 10^{-6}$ is added to model the array dynamics seen in the matched filter output. This is to model the internode range of the system as a constant value with a small, random perturbation to account for both positive and negative radial motions at random time instances. The experiments in the following section have induced motion that is proportional to the wavelength of the 1.5 GHz coherent frequency (20 cm), which is roughly 2% of

the sampling interval of the matched filter at 25 MHz (12 m). Since this induced motion is very small compared to the discretization of the matched filter, this acts like a fluctuation on an otherwise constant value and therefore a 1-D Kalman filter is sufficient. However, if the motion is much larger than a fraction of the matched filter sampling rate, resulting in discontinuities in the matched filter output, the Kalman filter will diverge. If this is the case other techniques such as a higher dimensional Kalman filter to measure velocity and acceleration, such as an extended Kalman filter (EKF) [46]–[48] to linearize the discontinuities or an unscented Kalman filter (UKF) [49]–[51], may be needed. The time delay estimate found from the output of the Kalman filter is converted to a phase shift of the operational frequency. This phase shift is then applied to the beamforming carrier signal on the secondary node. Thus, as the primary and secondary nodes change their relative positions, the outputs remain phase locked at the target location.

V. Distributed Antenna Array and Open-Loop Distributed Beamforming Experiments

The architecture investigated in this work is based on a single primary node and multiple secondary nodes. As the objective is to demonstrate the ability to simultaneously measure internode range between multiple nodes with sufficient accuracy to support beamforming, we use continuous-wave transmitted signals, and we lock the reference oscillators via cable. Wireless frequency alignment can be implemented in various ways for a fully wireless system [18]–[20]. An image of the block diagram of the primary and secondary nodes can be seen in Fig. 5 (a) and (b) respectively. Each node consisted of two Ettus X310 SDRs, each of which was connected to one host computer running Windows 7 with 32 GB of RAM via 10 GB Ethernet cables. The X310 SDRs utilized two UBX 160 daughterboards which have operational bandwidths from DC to 6 GHz with an instantaneous bandwidth of up to 160 MHz. These daughterboards support complex up- and down-conversion for in-phase and quadrature mixing as well as internal amplification equivalent to 30 dB and 33.5 dB for the transmit and receive sides, respectively. A block diagram of the X310 RF chain can be seen in Fig. 6. The SDRs interfaced with the host computer using using LabVIEW 2018 where a maximum sampling rate of 25 MHz was possible which was limited by the data throughput between LabVIEW and the SDRs, restricting the maximum achievable instantaneous single-sideband bandwidth to 12.5 MHz.

One SDR on each node transmitted the signal for distributed beamforming. The second SDR was used to either implement ranging to the primary node, or, on the primary node, to capture and retransmit any incoming ranging signals from the secondary nodes. Each secondary node transmits a version of the ranging waveform with a distinct stepped-frequency pattern. The primary node repeats any incoming signals in a continuous manner (i.e. no time scheduling was required). Each secondary node then processes the received signal via matched filter followed by the Kalman filter refinement step. The experiments described below yielded SNR values of

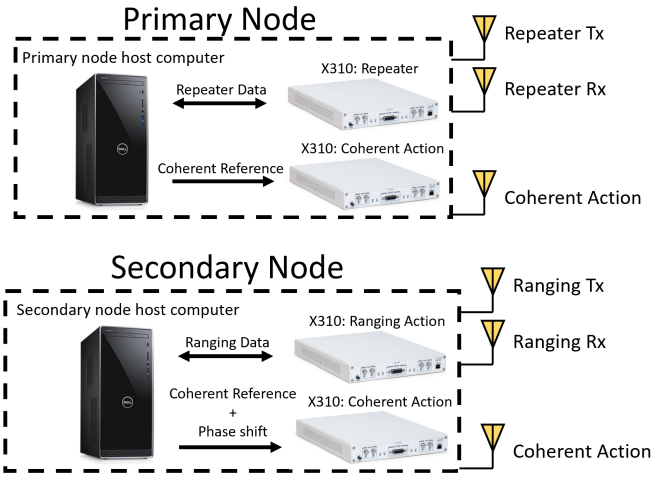

Fig. 5. Block diagrams of the nodes used in the experimental system.

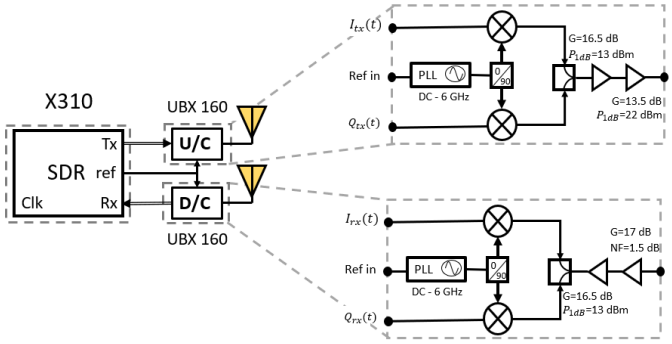

Fig. 6. RF chain internal to each of the X310 SDRs. Clk: clock. Tx: transmit. Rx: receive. U/C: upconverter. D/C: downconverter. PLL: phase locked-loop. G: gain. NF: noise figure.

approximately 30 dB, which were determined using an eigenvalue decomposition approach [33], [52]. The secondary nodes then calculate the range, from which the relative phase of the beamforming carrier frequency was updated based on (7).

The beamforming signals were transmitted from each node at a carrier frequency of 1.5 GHz using 1.35-9.5 GHz ultra wideband log periodic antennas. Transmission of the ranging signals from the secondary nodes was implemented at a carrier frequency of 4.25 GHz and after reception at the primary node, the ranging waveforms were retransmitted at a carrier frequency of 5.25 GHz, providing frequency diversity to mitigate the crosstalk and multipath. The beamformed signals were captured on a Keysight MSO-X 92004A oscilloscope. The levels of the individual signals were also recorded at each location by selectively turning on individual transmitters.

We implemented the ranging method in a three-node open-loop beamforming system. To our knowledge, this was the first open-loop distributed beamforming demonstration with more than two transmitting nodes. The array was oriented in an end-fire configuration, again to demonstrate the most challenging beamforming case. The setup is shown in the diagram of Fig. 7(a), where the red colored signals indicate the ranging signals and the blue signals represent the beamforming signals.

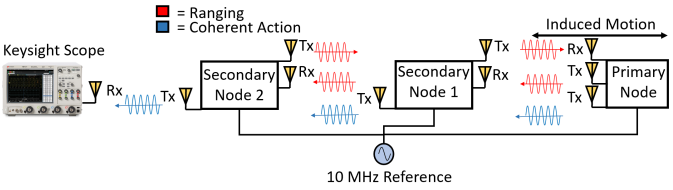

(a)

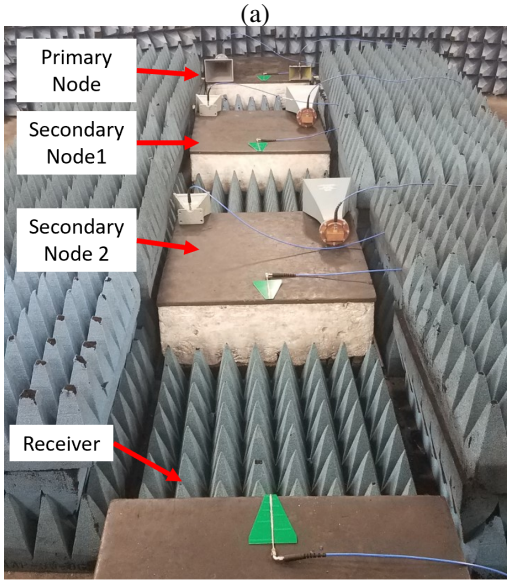

(b)

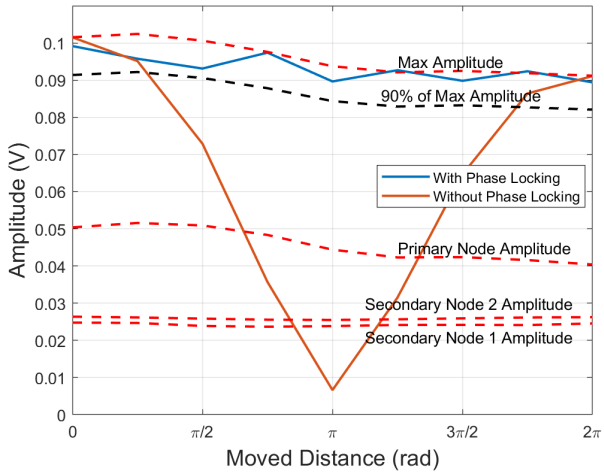

(c)

Fig. 7. (a) Block diagram of the distributed three-node experiment. (b) Image of the experimental setup in the semi-enclosed arch range. (c) Measured results showing the beamforming performance with and without performing range-based phase correction.

Fig. 7(b) shows the experimental system in a semi-anechoic chamber in the laboratory. The two secondary nodes were separated by 0.6 m, with first secondary node at a distance of 1 m from the receiving antenna. The primary node started at a distance of 1 m from the second secondary node. The two secondary nodes were stationary, and transmitted signals to the primary node, which captured, amplified, and retransmitted back these signals. No time scheduling was used for the two secondary nodes; the stepped-frequency waveform supported simultaneous multinode operation thus no scheduling was required. The primary node was moved in 2.5 cm increments for a total range of 20 cm. At each distance, 100 snapshots containing fifteen cycles of the 1.5 GHz signal were captured. The resulting 1,500 peak values were again averaged to give the measured amplitude at each distance.

The measured results of the three-node experiment are shown in Fig. 7(c). Here the two secondary nodes' individual amplitudes were constant since the secondary nodes were stationary. The uncorrected beamforming measurement showed a clear null, dropping to 7% of the total achievable amplitude when the primary node was in a location causing destructive interference. When the ranging system was utilized, the system maintained a high-gain beamforming signal, achieving coherent gain consistently above the 90% threshold, with average coherent gain above 95%.

TABLE I
COMPARISON OF DISTRIBUTED TRANSMIT BEAMFORMING DEMONSTRATIONS CONSISTING OF $N > 2$ TRANSMITTING NODES.

Method	Frequency	BF/C[a]	Coherent Gain[b]	Ref.
Closed-loop	900 MHz	100%[c]	$\approx$ 74%	[24]
Closed-loop	964 MHz	100%[c]	$>$ 95%	[25]
Retrodirective	910 MHz	99.95%	$>$ 97%	[27]
Retrodirective	915 MHz	$\approx$ 4%	$>$ 90% & 97%	[29]
Open-Loop	**1500 MHz**	**100%**[c]	$>$ **95%**	**This work**

[a] Beamforming duration per cycle.
[b] Average value for amplitude coherent gain.
[c] Separate band(s) used for synchronization.

VI. Conclusion

Distributed beamforming in open-loop systems requires scalable, high-accuracy coordination. Internode range estimation represents one of the fundamental coordination tasks necessary for open-loop beamforming, and is arguably the most challenging considering the error tolerances for microwave and millimeter-wave systems. The approach demonstrated in this work utilizes time of flight estimations whose accuracy was maximized by a one dimensional Kalman filter to enable real time dynamic phase adjustments for mobile open-loop beamforming arrays. Using this approach, multinode beamforming on platforms with relative motion was demonstrated without receiver feedback. This method provides a solution for scalable, high-accuracy localization that can support distributed beamforming between multiple nodes at transmission frequencies relevant for numerous wireless applications. Combined with wireless frequency synchronization and time alignment, fully open-loop distributed beamforming will be possible on future distributed wireless systems.

References

[1] F. K. Sharifabad, M. A. Jensen, and A. L. Anderson, "Array beamforming synthesis for point-to-point mimo communication," *IEEE Trans. Antennas Propag.*, vol. 63, no. 9, pp. 3878–3886, Sep. 2015.
[2] M. A. Jensen and J. W. Wallace, "A review of antennas and propagation for mimo wireless communications," *IEEE Trans. Antennas Propag.*, vol. 52, no. 11, pp. 2810–2824, Nov 2004.

[3] M. D. Migliore, "On the role of the number of degrees of freedom of the field in mimo channels," *IEEE Trans. Antennas Propag.*, vol. 54, no. 2, pp. 620–628, Feb 2006.

[4] F. K. Sharifabad, M. A. Jensen, J. Medbo, and J. Furuskog, "Measurement-based performance analysis of cooperative mimo beamforming," *IEEE Antennas Wireless Propag. Lett.*, vol. 11, pp. 1394–1397, 2012.

[5] M. Hefnawi, "Large-scale multi-cluster mimo approach for cognitive radio sensor networks," *IEEE Sensors Journal*, vol. 16, no. 11, pp. 4418–4424, 2016.

[6] W.-Q. Wang, "Phased-mimo radar with frequency diversity for range-dependent beamforming," *IEEE Sensors Journal*, vol. 13, no. 4, pp. 1320–1328, 2012.

[7] F. I. Urzaiz, J. Gismero-Menoyo, A. Asensio-López, and Á. D. de Quevedo, "Digital beamforming on receive array calibration: Application to a persistent x-band surface surveillance radar," *IEEE Sensors Journal*, vol. 21, no. 5, pp. 6752–6760, 2020.

[8] S. Jayaprakasam, S. K. Abdul Rahim, C. Y. Leow, T. O. Ting, and A. A. Eteng, "Multiobjective beampattern optimization in collaborative beamforming via nsga-ii with selective distance," *IEEE Trans. Antennas Propag.*, vol. 65, no. 5, pp. 2348–2357, May 2017.

[9] R. Mudumbai, G. Barriac, and U. Madhow, "On the feasibility of distributed beamforming in wireless networks," *IEEE Transactions on Wireless Communications*, vol. 6, no. 5, pp. 1754–1763, May 2007.

[10] D. C. Jenn, "Transmission equation for multiple cooperative transmitters and collective beamforming," *IEEE Antennas Wireless Propag. Lett.*, vol. 7, pp. 606–608, 2008.

[11] Y. Fan, Y. Zhou, D. He, and W. Xia, "Fast transmit beamforming with distributed antennas," *IEEE Antennas Wireless Propag. Lett.*, vol. 16, pp. 121–124, 2017.

[12] J. C. Kwan and A. O. Fapojuwo, "Performance optimization of a multi-source, multi-sensor beamforming wireless powered communication network with backscatter," *IEEE Sensors Journal*, vol. 19, no. 22, pp. 10 898–10 909, 2019.

[13] S. Goguri, D. Ogbe, S. Dasgupta, R. Mudumbai, D. R. Brown, D. J. Love, and U. Madhow, "Optimal precoder design for distributed transmit beamforming over frequency-selective channels," *IEEE Trans. Wireless Commun.*, vol. 17, no. 11, pp. 7759–7773, Nov 2018.

[14] M. Rossi, A. M. Haimovich, and Y. C. Eldar, "Spatial compressive sensing for mimo radar," *IEEE Trans. Signal Process.*, vol. 62, no. 2, pp. 419–430, Jan 2014.

[15] C. Chen, C. Tseng, J. Denis, and C. Lin, "Adaptive distributed beamforming for amplify-and-forward relay networks: Convergence analysis," *IEEE Transactions on Wireless Communications*, vol. 13, no. 8, pp. 4167–4178, Aug 2014.

[16] J. A. Nanzer, R. L. Schmid, T. M. Comberiate, and J. E. Hodkin, "Open-loop coherent distributed arrays," *IEEE Transactions on Microwave Theory and Techniques*, vol. 65, no. 5, pp. 1662–1672, May 2017.

[17] H. Ouassal, T. Rocco, M. Yan, and J. A. Nanzer, "Decentralized frequency synchronization in distributed antenna arrays with quantized frequency states and directed communications," *IEEE Transactions on Antennas and Propagation*, pp. 1–1, 2020.

[18] T. Musch, M. Gerding, and B. Schiek, "A phase-locked-loop concept for the generation of two rf-signals with a small frequency offset," *IEEE Transactions on Instrumentation and Measurement*, vol. 54, no. 2, pp. 709–712, April 2005.

[19] W. Chiu, Y. Huang, and T. Lin, "A dynamic phase error compensation technique for fast-locking phase-locked loops," *IEEE Journal of Solid-State Circuits*, vol. 45, no. 6, pp. 1137–1149, June 2010.

[20] S. Mghabghab, H. Ouassal, and J. A. Nanzer, "Wireless frequency synchronization for coherent distributed antenna arrays," in *2019 IEEE International Symposium on Antennas and Propagation and USNC-URSI Radio Science Meeting*, July 2019, pp. 1575–1576.

[21] C. Shen and H. Yu, "Time-delay alignment technique for a randomly distributed sensor array," *IET Communications*, vol. 5, no. 8, pp. 1068–1072, May 2011.

[22] P. Chatterjee and J. A. Nanzer, "Effects of time alignment errors in coherent distributed radar," in *2018 IEEE Radar Conference (RadarConf18)*, April 2018, pp. 0727–0731.

[23] ——, "Sdr-based wireless time alignment for coherent distributed beamforming," in *2019 USNC-URSI Radio Science Meeting*, July 2019.

[24] M. M. Rahman, H. E. Baidoo-Williams, R. Mudumbai, and S. Dasgupta, "Fully wireless implementation of distributed beamforming on a software-defined radio platform," in *Proceedings of the 11th international conference on Information Processing in Sensor Networks*, 2012, pp. 305–316.

[25] F. Quitin, M. M. U. Rahman, R. Mudumbai, and U. Madhow, "A scalable architecture for distributed transmit beamforming with commodity radios: Design and proof of concept," *IEEE Transactions on Wireless Communications*, vol. 12, no. 3, pp. 1418–1428, 2013.

[26] W. Tushar and D. B. Smith, "Distributed transmit beamforming based on a 3-bit feedback system," in *2010 IEEE 11th International Workshop on Signal Processing Advances in Wireless Communications (SPAWC)*, June 2010, pp. 1–5.

[27] P. Bidigare, M. Oyarzyn, D. Raeman, D. Chang, D. Cousins, R. O'Donnell, C. Obranovich, and D. R. Brown, "Implementation and demonstration of receiver-coordinated distributed transmit beamforming across an ad-hoc radio network," in *2012 Conference Record of the Forty Sixth Asilomar Conference on Signals, Systems and Computers (ASILOMAR)*, Nov 2012, pp. 222–226.

[28] B. Peiffer, R. Mudumbai, A. Kruger, A. Kumar, and S. Dasgupta, "Experimental demonstration of a distributed antenna array pre-synchronized for retrodirective transmission," in *2016 Annual Conference on Information Science and Systems (CISS)*, March 2016, pp. 460–465.

[29] B. Peiffer, R. Mudumbai, S. Goguri, A. Kruger, and S. Dasgupta, "Experimental demonstration of retrodirective beamforming from a fully wireless distributed array," in *MILCOM 2016 - 2016 IEEE Military Communications Conference*, 2016, pp. 442–447.

[30] D. R. Brown III and H. V. Poor, "Time-slotted round-trip carrier synchronization for distributed beamforming," *IEEE Transactions on Signal Processing*, vol. 56, no. 11, pp. 5630–5643, Nov 2008.

[31] R. D. Preuss and D. R. Brown, III, "Two-way synchronization for coordinated multicell retrodirective downlink beamforming," *IEEE Transactions on Signal Processing*, vol. 59, no. 11, pp. 5415–5427, Nov 2011.

[32] T. M. Comberiate, R. L. Schmid, J. E. Hodkin, M. D. Sharp, and J. A. Nanzer, "A bandpass sampling receiver for wide-bandwidth, spectrally-sparse waveforms for high-accuracy range measurements," *IEEE Microwave and Wireless Components Letters*, vol. 27, no. 1, pp. 88–90, Jan 2017.

[33] S. M. Ellison, S. Mghabghab, J. J. Doroshewitz, and J. A. Nanzer, "Combined wireless ranging and frequency transfer for internode coordination in open-loop coherent distributed antenna arrays," *IEEE Transactions on Microwave Theory and Techniques*, vol. 68, no. 1, pp. 277–287, Jan 2020.

[34] L. Hu, S. Zhang, and G. Lu, "Observation-to-track pairing using electro-optical(eo) systems," in *2006 International Conference on Mechatronics and Automation*, June 2006, pp. 589–594.

[35] S. C. Taylor, "High-precision tracking: an essential component of the optical multiple access (oma) system," in *IEE Colloquium on Optical Intersatellite Links and On-Board Techniques*, Jan 1990, pp. 12/1–12/7.

[36] J. Jason, H.-E. Nilsson, B. Arvidsson, and A. Larsson, "Experimental study of an intensity modulated fiber-optic position sensor with a novel readout system," *IEEE Sensors Journal*, vol. 8, no. 7, pp. 1105–1113, 2008.

[37] S. M. Ellison and J. A. Nanzer, "High-accuracy multi-node ranging for coherent distributed antenna arrays," *IEEE Transactions on Aerospace and Electronic Systems*, pp. 1–1, 2020.

[38] F. Alsubaie, "Multiple signal classification for determining direction of arrival of frequency hopping spread spectrum signals," Master's thesis, Air Force Institute of Technology, Wright-Patterson Air Force Base, 2014.

[39] R. Schmidt, "Multiple emitter location and signal parameter estimation," *IEEE Transactions on Antennas and Propagation*, vol. 34, no. 3, pp. 276–280, 1986.

[40] R. Roy and T. Kailath, "Esprit-estimation of signal parameters via rotational invariance techniques," *IEEE Transactions on acoustics, speech, and signal processing*, vol. 37, no. 7, pp. 984–995, 1989.

[41] J. A. Nanzer and M. D. Sharp, "On the estimation of angle rate in radar," *IEEE Transactions on Antennas and Propagation*, vol. 65, no. 3, pp. 1339–1348, March 2017.

[42] A. Schlegel, S. M. Ellison, and J. A. Nanzer, "A microwave sensor with submillimeter range accuracy using spectrally sparse signals," *IEEE Microwave and Wireless Components Letters*, vol. 30, no. 1, pp. 120–123, Jan 2020.

[43] K. S. Zilevu, J. E. Hodkin, M. D. Sharp, T. M. Comberiate, and J. A. Nanzer, "Waveforms and signal processing for high-accuracy microwave metrology," in *2015 IEEE International Symposium on Antennas and Propagation USNC/URSI National Radio Science Meeting*, July 2015, pp. 977–978.

[44] J. A. Nanzer, M. D. Sharp, and D. R. Brown, "Bandpass signal design for passive time delay estimation," in *Signals, Systems and Computers, 2016 50th Asilomar Conference on*. IEEE, 2016, pp. 1086–1091.

[45] R. E. Kalman, "A new approach to linear filtering and prediction problems," *Journal of basic Engineering*, vol. 82, no. 1, pp. 35–45, 1960.
[46] S. J. Julier and J. K. Uhlmann, "Unscented filtering and nonlinear estimation," *Proceedings of the IEEE*, vol. 92, no. 3, pp. 401–422, March 2004.
[47] A. H. Jazwinski, *Stochastic processes and filtering theory*. Courier Corporation, 2007.
[48] H. W. Sorenson, *Kalman filtering: theory and application*. IEEE, 1985.
[49] S. J. Julier and J. K. Uhlmann, "New extension of the kalman filter to nonlinear systems," in *Signal processing, sensor fusion, and target recognition VI*, vol. 3068. International Society for Optics and Photonics, 1997, pp. 182–193.
[50] S. J. Julier, "The scaled unscented transformation," in *Proceedings of the 2002 American Control Conference (IEEE Cat. No.CH37301)*, vol. 6, May 2002, pp. 4555–4559 vol.6.
[51] E. A. Wan and R. Van Der Merwe, "The unscented kalman filter for nonlinear estimation," in *Proceedings of the IEEE 2000 Adaptive Systems for Signal Processing, Communications, and Control Symposium (Cat. No. 00EX373)*. Ieee, 2000, pp. 153–158.
[52] M. Hamid, N. Björsell, and S. B. Slimane, "Sample covariance matrix eigenvalues based blind snr estimation," in *2014 IEEE International Instrumentation and Measurement Technology Conference (I2MTC) Proceedings*, May 2014, pp. 718–722.